Proceedings World Geothermal Congress 2000
Kyushu - Tohoku, Japan, May 28 - June 10, 2000

DEVELOPMENT OF NUMERICAL SIMULATION CODE FOR HYDRAULIC FRACTURING USING EMBEDDED CRACK ELEMENT

Kazushi Sato[1] and Toshiyuki Hashida[2]
[1]Miyagi National College of Technology, 48 Aza-Nodayama, Shiote, Medeshima, Natori, Japan
[2]Fracture Research Institute, Tohoku University, 01 Aza-Aoba, Aramaki, Aobaku, Sendai, Japan

Key Words: Hydraulic Fracturing, Numerical Analysis, Embedded Crack Element, Mixed-Mode Fracture

ABSTRACT

Hydraulically driven fracture propagation in rock may occur in mixed mode (Mode I and II). The purpose of this study is the development of the numerical simulation code that can predict a mixed mode crack propagation with a fracture process zone during hydraulic fracturing in a deep rock mass. A finite element analysis with an embedded crack element is adopted to the simulation code. The embedded crack element represents a crack as a displacement discontinuity within a continuum element. A crack constitutive model for mixed mode fracture is incorporated into the embedded crack element. The results from single element calculation indicate that the softening behaviour is reproduced in tension and shear mode, and the dilational behaviour during shear slip is captured. The analysis of hydraulic fracturing demonstrates that the mixed mode cracking is reproduced.

1. INTRODUCTION

Hydraulically driven fracture propagation in rock may occur in mixed mode (Mode I and II). In order to predict the mixed mode crack propagation, the direction of the propagating crack must be analyzed. Furthermore, the crack growth is accompanied by a formation of fracture process zone, so that the prediction becomes more difficult.

The purpose of this study is the development of a numerical simulation code that can predict a mixed mode crack propagation with a fracture process zone during hydraulic fracturing in a deep rock mass. In order to handle both an arbitrary crack geometry, due to the mixed mode crack growth, and formation of the fracture process zone, a finite element analysis with an embedded crack (EC) representation is adopted.

The EC approach has been proposed (Dvorkin et al., 1990; Klisinski et al., 1991; Lotfi and Shing, 1995; Ohlsson and Olofsson, 1997) to deal with the strong displacement localization such as crack and/or shear bands in quasi-brittle materials. In the EC element, a crack is modelled as a displacement discontinuity within a continuum element. The major advantage of the EC approach is that discrete cracks can be introduced anywhere and in any direction within the finite element mesh. Also, a cohesive crack model can be implemented as a constitutive law for the embedded crack.

This paper presents the fundamental formulation of EC element based on that by Lotfi and Shing (1995) and adapting a crack constitutive model for mixed mode fracture into the EC element.

2. EMBEDDED CRACK ELEMENT

The formulation of EC element by Lotfi and Shing (1995) is used in this study. In this formulation, any crack constitutive model can be adopted to represent the behaviour of the internal displacement discontinuity.

In this section, a brief description of the EC element formulation and the mixed-mode crack constitutive model which is adopted into the EC element is presented.

2.1 Element Formulation

The plane strain condition and an elastic body with an inelastic interface representing a crack is assumed.

The principle of virtual work for a body with an internal interface, as shown in Figure 1, can be expressed as

$$\int_V (\nabla \delta\mathbf{u})^{\mathrm{T}} \boldsymbol{\sigma}\, \mathrm{d}V - \int_V \delta\mathbf{u}^{\mathrm{T}} \hat{\mathbf{b}}\, \mathrm{d}V - \int_{S_t} \delta\mathbf{u}^{\mathrm{T}} \hat{\mathbf{t}}\, \mathrm{d}S + \int_{S_d} (\delta\mathbf{u}^{+} - \delta\mathbf{u}^{-})^{\mathrm{T}} \mathbf{t}_d\, \mathrm{d}S = 0 \tag{1}$$

where $\boldsymbol{\sigma}$ is a stress vector consisting of three stress components in the continuous body V^+ and V^-, in which + and – refer to the positive and negative side of the interface, $\hat{\mathbf{b}}$ is a body force vector, $\hat{\mathbf{t}}$ is a prescribed traction vector on the boundary S_t, and $\mathbf{t}_\mathrm{d}$ is a traction vector on the internal interface S_d. The displacement vector $\mathbf{u}$ is continuous within V^+ and V^-, however it is discontinuous across S_d. For an inelastic interface, $\mathbf{t}_\mathrm{d}$ is a function of the relative displacement between the opposite faces of the interface, i.e. $\mathbf{u}^+ - \mathbf{u}^-$. For the finite element formulation, the displacement field is approximated as

$$\mathbf{u} = \mathbf{N}_u \bar{\mathbf{u}} + \mathbf{N}_d \bar{\mathbf{d}} \tag{2}$$

where $\mathbf{N}_u$ is an element shape function, $\mathbf{N}_d$ is a discontinuous shape function, $\bar{\mathbf{u}}$ is a nodal displacement vector and $\bar{\mathbf{d}}$ is a interface deformation vector. In equation (2), $\mathbf{N}_d\bar{\mathbf{d}}$ is a discontinuous distortion in the continuous displacement field approximation $\mathbf{N}_u\bar{\mathbf{u}}$. The value of $\mathbf{N}_d\bar{\mathbf{d}}$ vanishes at the nodes. With the above approximation, the relative displacement field $\mathbf{d}$ along the internal interface is obtained as

$$\mathbf{d} = \mathbf{u}^+ - \mathbf{u}^- \approx (\mathbf{N}_d^+ - \mathbf{N}_d^-)\bar{\mathbf{d}} \tag{3}$$

Different deformation modes of the internal interface can be taken into account, depending on the discontinuous shape function. The derivation of the discontinuous shape function is described later in this section.

From the displacement field approximation of equation (2), $\nabla\mathbf{u}$ can be expressed as

$$\nabla \mathbf{u} \approx \mathbf{B}_u \bar{\mathbf{u}} + \mathbf{B}_d \bar{\mathbf{d}} \tag{4}$$

in which $\mathbf{B}_u = \mathbf{L}\mathbf{N}_u$ is the usual strain-displacement matrix, where $\mathbf{L}$ is the differential operator, and $\mathbf{B}_d = \mathbf{L}\mathbf{N}_d$. Discretizing equation (1) using equations (2)–(4), the following system equations are obtained

$$\int_V \mathbf{B}_u^{\mathrm{T}} \sigma dV = \mathbf{f}_u \tag{5a}$$

$$\int_V \mathbf{B}_d^{\mathrm{T}} \sigma dV + \int_{S_d} (\mathbf{N}_d^+ - \mathbf{N}_d^-)^{\mathrm{T}} \mathbf{t}_d dS = \mathbf{f}_d \tag{5b}$$

where $\mathbf{f}_u$ and $\mathbf{f}_d$ are defined as

$$\mathbf{f}_u = \int_V \mathbf{N}_u^{\mathrm{T}} \hat{\mathbf{b}} dV + \int_{S_t} \mathbf{N}_u^{\mathrm{T}} \hat{\mathbf{t}} dS \tag{6}$$

$$\mathbf{f}_d = \int_V \mathbf{N}_d^{\mathrm{T}} \hat{\mathbf{b}} dV + \int_{S_t} \mathbf{N}_d^{\mathrm{T}} \hat{\mathbf{t}} dS \tag{7}$$

For a simulation of hydraulic fracturing, $\mathbf{t}_d$ in equation (5b) is replaced by $\mathbf{t}_d$–$\mathbf{p}$, in which $\mathbf{p}$ is the vector of hydraulic pressure acting onto the crack surface. Thus, equation (5b) is modified to

$$\int_V \mathbf{B}_d^{\mathrm{T}} \sigma dV + \int_{S_d} (\mathbf{N}_d^+ - \mathbf{N}_d^-)^{\mathrm{T}} \mathbf{t}_d dS = \mathbf{f}_d + \int_{S_d} (\mathbf{N}_d^+ - \mathbf{N}_d^-)^{\mathrm{T}} \mathbf{p} dS \,. \tag{5b'}$$

For linear elastic material, the constitutive equation can be expressed in a rate form as

$$\dot{\sigma} = \mathbf{D}(\mathbf{B}_u \dot{\bar{\mathbf{u}}} + \mathbf{B}_d \dot{\bar{\mathbf{d}}}) \tag{8}$$

in which $\mathbf{D}$ is the elastic stiffness matrix. Similarly, for a non-linear interface, the constitutive equation in rate form is expressed as

$$\dot{\mathbf{t}}_d = \mathbf{D}_d \dot{\mathbf{d}} \approx \mathbf{D}_d (\mathbf{N}_d^+ - \mathbf{N}_d^-) \dot{\bar{\mathbf{d}}} \tag{9}$$

where $\mathbf{D}_d$ is the interface stiffness. With these definitions, the rate form equation of the system equations (5a), (5b) is

$$\begin{bmatrix} \mathbf{K}_{uu} & \mathbf{K}_{ud} \\ \mathbf{K}_{ud}^{\mathrm{T}} & \mathbf{K}_{dd} + \mathbf{K}_d \end{bmatrix} \begin{bmatrix} \dot{\bar{\mathbf{u}}} \\ \dot{\bar{\mathbf{d}}} \end{bmatrix} = \begin{bmatrix} \dot{\mathbf{f}}_u \\ \dot{\mathbf{f}}_d \end{bmatrix} \tag{10}$$

in which

$$\mathbf{K}_{uu} = \int_V \mathbf{B}_u^{\mathrm{T}} \mathbf{D} \mathbf{B}_u dV \tag{11}$$

$$\mathbf{K}_{ud} = \int_V \mathbf{B}_u^{\mathrm{T}} \mathbf{D} \mathbf{B}_d dV \tag{12}$$

$$\mathbf{K}_{dd} = \int_V \mathbf{B}_d^{\mathrm{T}} \mathbf{D} \mathbf{B}_d dV \tag{13}$$

$$\mathbf{K}_d = \int_{S_d} (\mathbf{N}_d^+ - \mathbf{N}_d^-)^{\mathrm{T}} \mathbf{D}_d (\mathbf{N}_d^+ - \mathbf{N}_d^-) dS \tag{14}$$

The discontinuity shape function $\mathbf{N}_d$ is defined as

$$\mathbf{N}_d = \mathbf{M}_0 - \mathbf{N}_u \mathbf{P}_0 \tag{15}$$

under the assumption of a uniform deformation field along the internal interface. In equation (15), $\mathbf{M}_0 = M\mathbf{I}$, where $\mathbf{I}$ is a identity matrix, M is a constant discontinuity function expressed as

$$M = \begin{cases} \alpha & (\text{in } V^+) \\ \alpha - 1 & (\text{in } V^-) \end{cases} \tag{16}$$

where $0 \le \alpha \le 1$, and $\mathbf{P}_0$ is given by

$$\mathbf{P}_0 = \begin{bmatrix} M_1\mathbf{I} & M_2\mathbf{I} & .... & M_{n_{node}}\mathbf{I} \end{bmatrix}^{\mathrm{T}} \tag{17}$$

in which $M_i = M$ at node i and n_{node} is the number of nodes in the element. It should be noted that, when a uniform deformation is considered, the specific value of α does not affect the element formulation and can be set to any value between 0 and 1. In this study, α is set to be 0.5.

From equation (15)

$$\mathbf{B}_d = -\mathbf{B}_u \mathbf{P}_0 \tag{18}$$

is obtained. The evaluation of the integrals in the above system and rate equations becomes the same as that in continuum elements.

By considering out $\bar{\mathbf{d}}$ in equation (10),

$$\mathbf{K} \dot{\bar{\mathbf{u}}} = \dot{\mathbf{F}} \tag{19}$$

where

$$\mathbf{K} = \mathbf{K}_{uu} - \mathbf{K}_{uu} \mathbf{P}_0 (\mathbf{P}_0^{\mathrm{T}} \mathbf{K}_{uu} \mathbf{P}_0 + \mathbf{K}_d)^{-1} \mathbf{P}_0^{\mathrm{T}} \mathbf{K}_{uu} \tag{20}$$

and

$$\dot{\mathbf{F}} = \dot{\mathbf{f}}_u + \mathbf{K}_{uu} \mathbf{P}_0 (\mathbf{P}_0^{\mathrm{T}} \mathbf{K}_{uu} \mathbf{P}_0 + \mathbf{K}_d)^{-1} \dot{\mathbf{f}}_d \tag{21}$$

is obtained. $\mathbf{K}_{uu}$ is the stiffness matrix of an intact element. The nodal displacement vector $\bar{\mathbf{u}}$ is given by solving equation (19) at the structural level. After this, the interface deformation vector $\bar{\mathbf{d}}$ can be determined from the non-linear equation (5b) at the element level, then the stress vector $\boldsymbol{\sigma}$ is computed. Subsequently, the left hand side of equation (5a) is used for the assembly of internal force vectors.

A four node isoparametric element with internal interface based on the above formulation was used in this study. The condensed stiffness matrix $\mathbf{K}$ can be used for the iterations at the structural level. However, in the numerical examples presented in this paper, an initial stiffness matrix was used for the iterative solution.

2.2 Crack Constitutive Model

As mentioned above, any crack constitutive model can be adopted to represent the behaviour of the internal interface. The crack constitutive model is used to solve equation (5b) and also to determine which element should be switched from an intact element to an EC element, i.e. the crack initiation in the element at the initial state of the crack constitutive model.

The following failure function (Cervenka, 1994; Carol et al., 1998) is employed to express the behaviour of the crack

$$F = \tau^2 - (c - \sigma \tan\phi_f)^2 + (c - \sigma_T \tan\phi_f)^2 \qquad (22)$$

where τ and σ are the tangential and normal stress on the crack surface, respectively, c is the cohesion, ϕ_f is the angle of friction and σ_T is the tensile strength. A general shape of the failure function is shown in Figure 2. c and σ_T are functions of a softening parameter d_{eff} which is given by

$$d_{eff} = (d_t^2 + d_n^2)^{1/2} \qquad (23)$$

where d_t and d_n are, respectively, the tangential and normal relative displacement of the crack surface. The functions of c and σ_T represent softening behaviour in shear (Mode II) and tension (Mode I) as shown in Figure 3. These curves are often referred to as slip-weakening and tension-softening curve. Tension-softening curve and slip-weakening curve can be determined, respectively, by conducting direct tension tests (Hillerborg, 1983) and compression tests (Rice and Cleary, 1980). With the cracking process, since the failure function shrinks toward the final shape of the failure function, the stresses on the crack surface decrease with crack deformation.

The cracking model is implemented by dividing it into a crack initiation part and a crack evolution part.

A crack initiates when the stress state in an intact element reaches the initial failure function of the condition F=0. The crack direction can be calculated from the tangent at the contact point of the failure function and the Mohr's circle. The crack is introduced at the element centroid upon crack initiation and only one crack is allowed in each element. If the crack initiation criterion is satisfied at the centroid of a neighboring element, the crack propagates into that element.

After the crack has been formed, the crack evolution behaviour is dealt with by the EC element through the constitutive equation (9). $\mathbf{D}_d$ can be determined based on the theory of plasticity. However, considering a shear dilation, $\mathbf{D}_d$, deduced by the theory of plasticity, becomes an unsymmetrical matrix. This would imply the need to store the full stiffness matrix on the structural level. This is clearly not an efficient approach since only few elements will be EC elements, and only a small portion of the structural stiffness matrix will be unsymmetrical. To avoid this problem, Cervenka (1994) has proposed the use of a secant stiffness matrix as follows

$$\mathbf{D}_d = \begin{bmatrix} K_t & 0 \\ 0 & K_n \end{bmatrix} \qquad (24)$$

where K_t is the tangential stiffness of the crack and K_n is the normal stiffness. If the crack is in tension, K_t and K_n can be determined from the secant modulus of the slip-weakening curve and the tension-softening curve as shown in Figure 3, respectively. In this case, the stiffness decreases with increasing deformation. If the crack is in compression, the crack is closed so that K_t and K_n remain constant at the each initial value K_{t0} and K_{n0}.

In order to reproduce the softening behaviour in the EC element using the secant stiffness matrix (24), the crack stresses, $\mathbf{t}_d$ in the EC element, can not be determined using only the constitutive equation (9), since the stiffness remains a positive value. Therefore, a correcting procedure of $\mathbf{t}_d$, so-called "constitutive driver", is incorporated into the solution procedure for equation (5b). The correction of $\mathbf{t}_d$ is performed by taking account of the shear dilation. The correcting procedure, schematically drawn in Figure 4, is as follows.

For a new nodal displacement, $\overline{\mathbf{u}}^{n+1}$, in which the superscript denotes the loading stage, when a new (tentative) crack deformation vector $\overline{\mathbf{d}}^{n+1}$ is determined by solving the 2nd row of equation (10), $\mathbf{t}_d^n$ moved to $\mathbf{t}_e$ based on the crack stiffness $\mathbf{D}_d$ and deformation increment. Since the new stress state $\mathbf{t}_d^{n+1}$ must satisfy $F^{n+1}=0$ determined by d_{eff}^{n+1}, $\mathbf{t}_e$ is returned back to the failure condition $F^{n+1}=0$. The direction of the return back vector for case 1 (see Figure 4) is normal to the shear dilation potential Q as

$$Q = \tau^2 - \sigma^2 \left(\frac{K_{n0}}{K_{t0}} \tan\phi_d \right)^2 \qquad (25)$$

where ϕ_d is the shear dilation angle. For the case 2, the direction is defined by connecting $\mathbf{t}_e$ with the origin. Subsequently, $\mathbf{t}_d^{n+1}$ is examined by equation (5b). Until equation (5b) is satisfied, the above procedure is repeated.

3. NUMERICAL EXAMPLES

3.1 Verification of Constitutive Driver

In order to verify the validity of the constitutive driver, simple calculations using one element were carried out. The element size is 10x10 mm.

The material properties used in this study are listed in Table 1. The tension-softening curve and the slip weakening curve used are shown in Figure 5 and 6, respectively.

Figure 7(a) illustrates a deformation mode and boundary conditions for a direct tension test. The computation was started from intact element, therefore, a crack was nucleated at the tensile strength. The load-displacement curve obtained from the calculation is indicated in Figure 8. As shown in Figure 8, the softening behaviour is reproduced.

Figure 7(b) illustrates a deformation mode and boundary conditions for a direct shear test. The crack was defined as input data to examine the slip behaviour of the interface. The result is indicated in Figure 9. The load-displacement curve shows a slip-weakening behaviour and the residual shear strength due to the friction. The tangential and normal displacement shown in Figure 9 is the relative displacement between the crack surfaces in each direction. The normal displacement indicates the shear dilation behaviour, which is defined by equation (25) with ϕ_d=20°. Since the maximum magnitude of shear dilation has been limited, the dilation becomes constant at 0.5 mm.

These results demonstrate the validity of the constitutive driver incorporated with the EC element.

3.2 Hydraulically Driven Fracture

A numerical computation of hydraulically driven fracture propagation was carried out. The finite element mesh

configuration is shown in Figure 10. The confining stresses are applied, 40 MPa in vertical direction and 20 MPa in horizontal direction. An initial crack, which is represented by two successive EC elements, is introduced as shown in Figure 10. This pre-defined crack is slanted 45° against the direction of the maximum confining stress, expecting a mixed mode cracking. The material properties are identical to those in the examples above.

In the calculation, since the fluid flow through the crack is not implemented, a simulating pressure is applied to the crack surfaces. When a crack nucleates during the calculation, if the new crack connects to the initial crack, the simulating pressure is adjusted from the initial pressure (200 MPa in this example) based on the volume of all connecting cracks, and the adjusted pressure is applied to the connecting cracks. Then, re-calculation is performed in the new pressure condition. Until no crack nucleation is achieved, the above procedure is iterated.

The final crack pattern with the finite element mesh is indicated in Figure 11. It is observed that the main crack advances from the initial crack, curving toward the direction of the maximum confining stress due to the mixed mode loading, and small isolated cracks are formed near the main crack. It seems that the cracking behaviour obtained from the calculation corresponds to the rock fracture behaviour. The crack pattern may depend on either the element size or the distortion of the element geometry. Lotfi and Shing (1995) indicate that the EC element is not sensitive to the mesh size and the mesh distortion, when the opening mode is dominant in the fracture mode. Though further studies should be done, it can be consider that the developed program code has a capability of analyzing a hydraulically driven fracture propagation in rock. Again, representing a complex geometry of cracks, as shown in Figure 11, without mesh refinement is the large advantage of the EC element.

4. CONCLUSION

In order to develop a numerical simulation code for hydraulic fracturing in deep rock mass, a crack constitutive model for mixed mode fracture was incorporated into the embedded crack element. The results from single element calculation indicate that the softening behaviour is reproduced in tension and shear mode, and the dilation behaviour during shear slip is captured. The analysis of hydraulic fracturing demonstrates that the mixed mode cracking is reproduced.

However, further development has to be done for a fluid flow through the crack and a flow within, and a deformation of, the rock mass.

ACKNOWLEDGMENTS

The study presented in this paper was supported by The Japan Society for the Promotion of Science under “Research for Future” program (JSPS-RFTF 97P00901), and The Ministry of Education, Science, Sports and Culture under Grant-in-Aid for Scientific Research (No. 10650068) and Grant-in-Aid for Encouragement of Young Scientists (No. 11750088).

REFERENCES

Carol, I., Prat, P. C. and López C. M. (1997). Normal/shear cracking model: application to discrete crack analysis. *J. Eng. Mech.*, Vol. 123(8), pp.765-773.

Cervenka, J. (1994). Discrete crack modeling in concrete structres, PhD thesis, Univ. of Colorado, Boulder.

Dvorkin, E. N., Cuitino, A. M. and Gioia, G. (1990). Finite elements with displacement interpolated embedded localization lines insensitive to mesh size and distortions. *Int. j. Numer. Methods. Eng.*, Vol. 30, pp.541-564.

Hillerborg, A. (1983). Analysis of one single crack, in: *Fracture Mechanics of Concrete*, F. H. Wittmann (Ed.)., Elsevier Science Publishers, B. V., Amsterdam, pp.223-250.

Klisinski, M., Runesson, K. and Sture S. (1991). Finite element with inner softening band. *J. Eng. Mech.*, Vol. 117(3), pp.575-587.

Lotfi, H. R. and Shing, B. (1995). Embedded representation of fracture in concrete with mixed finite elements. *Int. j. Numer. Methods. Eng.*, Vol. 38, pp.1307-1325.

Ohlsson, U. and Olofsson, T. (1997). Mixed-mode fracture and anchor bolts in concrete analysis with inner softening bands. *J. Eng. Mech.*, Vol. 123(10), pp.1027-1033.

Rice, J. R. and Cleary, M. P. (1976). Some basic stress diffusion solutions for fluid-saturated elastic porous media with compressible constituents. *Rev. Geophys. and Space Phys.*, Vol. 14, pp.227-241.

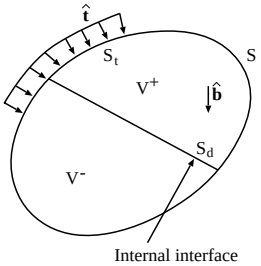

Figure 1. Continuum with internal interface.

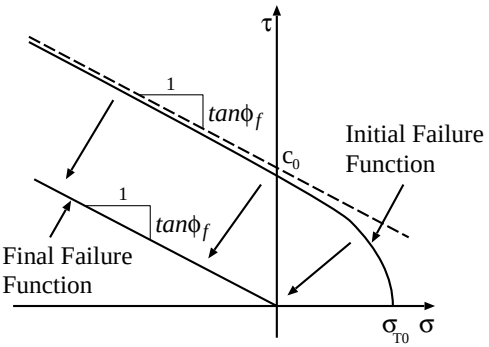

Figure 2. Failure function.

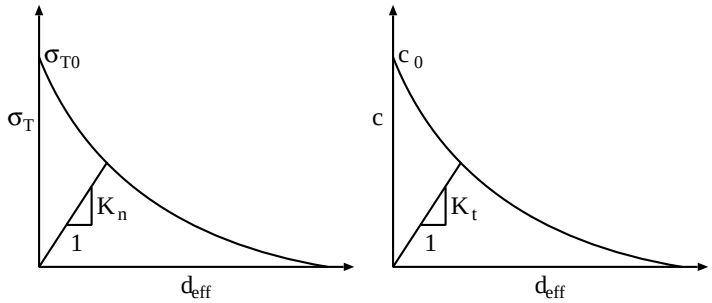

(a) Tension-softening curve (b) Slip-weakening curve

Figure 3. Softening behaviour.

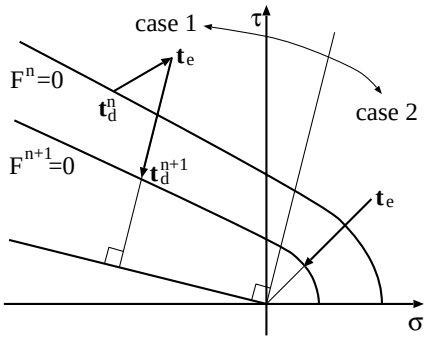

Figure 4. Definition of return direction.

Table 1. Material properties used.

Young's modulus	50 MPa
Poisson's ratio	0.25
Initial tensile strength	5.0 MPa
Initial cohesion	80 MPa
Friction angle	40 deg.
Shear dilation angle	20 deg.
Maximum dilatant displacement	0.5 mm

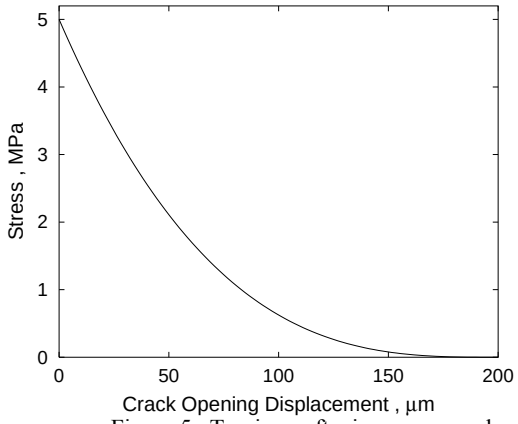

Figure 5. Tension-softening curve used.

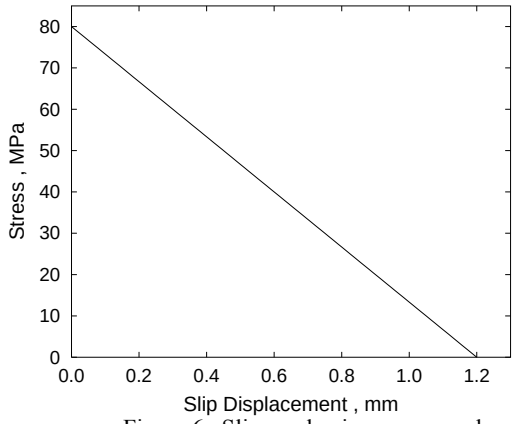

Figure 6. Slip-weakening curve used.

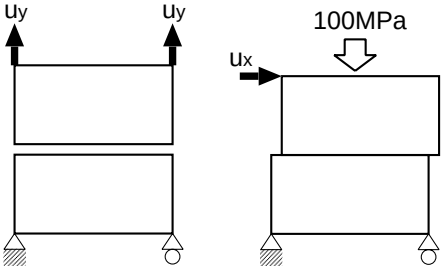

(a) direct tension (b) direct shear

Figure 7. Deformation mode.

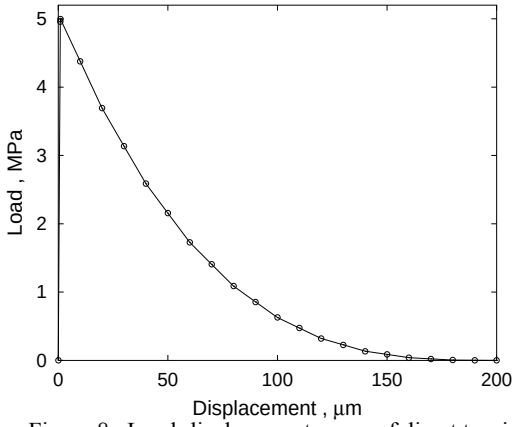

Figure 8. Load-displacement curve of direct tension test.

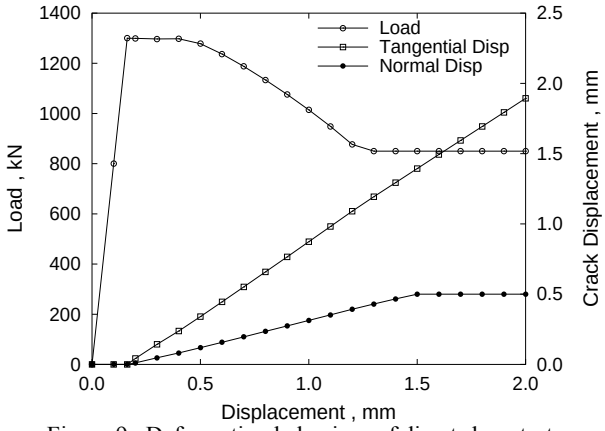

Figure 9. Deformation behaviour of direct shear test.

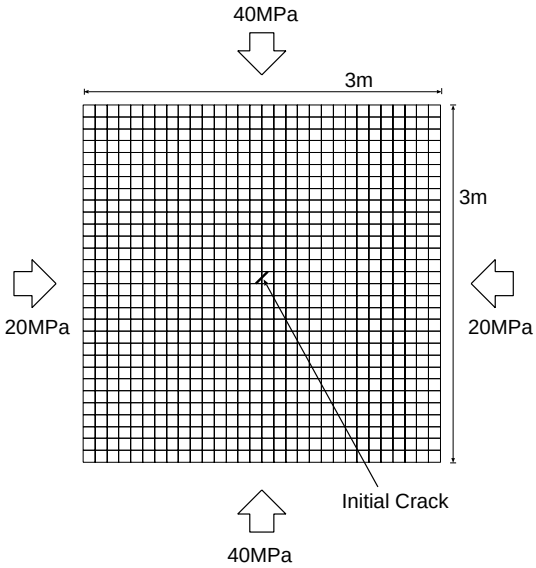

Figure 10. Finite element mesh used.

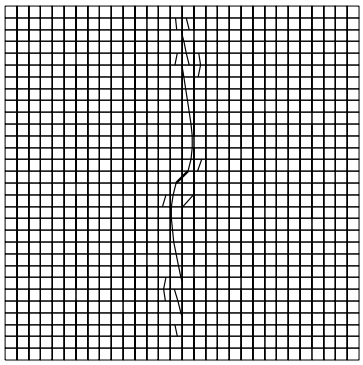

Figure 11 Final crack pattern.